JOURNAL OF Materials CHEMISTRY

Crystal structure, thermal and magnetic properties of $La_4Co_3O_9$. Phase relations for $La_4Co_3O_{10-\delta}$ ($0.00 \leqslant \delta \leqslant 1.00$) at 673 K

Ole Henrik Hansteen,[a] Helmer Fjellvåg*[a] and Bjørn C. Hauback[b]

[a] *Department of Chemistry, University of Oslo, N-0315 Oslo, Norway*
[b] *Institutt for energiteknikk, N-2007 Kjeller, Norway*

Phase relations and reoxidation behaviour is reported for samples with nominal composition $La_4Co_3O_{10-\delta}$ ($0.00 \leqslant \delta \leqslant 1.00$) synthesized by isothermal reduction at 673 K. The crystal structure of $La_4Co_3O_9$ has been determined on the basis of high-resolution powder X-ray diffraction and neutron diffraction data. The space group is *Pnma*, $a = 545.72$ pm, $b = 2855.3$ pm, $c = 565.42$ pm at RT; $R_{wp}(PXD) = 6.2\%$, $R_{wp}(PND) = 9.0\%$, $R_p(PXD) = 4.4\%$, $R_p(PND) = 7.0\%$. Reduction of $La_4Co_3O_{10}$ into $La_4Co_3O_9$ leads to ordering of oxygen vacancies. Chains of corner-sharing CoO_4 tetrahedra running along [100] are formed within the central-layer of each triple perovskite type layer of the Ruddlesden–Popper type structure of $La_4Co_3O_{10}$, whereas the top and bottom layers retain the perovskite type arrangement of corner-sharing CoO_6 octahedra. $La_4Co_3O_9$ orders antiferromagnetically at temperatures below $T_N = 303 \pm 5$ K. The magnetic structure is described on the basis of powder neutron diffraction data. The magnetic moments $\mu_{tet} = 2.6 \pm 0.1 \mu_B$ and $\mu_{oct} = 3.0 \pm 0.1 \mu_B$ correspond fairly well to spin only values for high-spin Co^{II}.

Introduction

Vacancy ordered phases are frequently formed upon low temperature ($T < 900$ K) reduction of transition metal perovskite type oxides,[1] *e.g.* $LaCoO_3$ reduces to $La_3Co_3O_8$ and $La_2Co_2O_5$.[2,3] Such phases are connected with a lower valence state for the transition metal component. $La_4Co_3O_{10}$ adopts the (layered) Ruddlesden–Popper type structure, belonging to the series $La_{m+1}Co_mO_{3m+1}$ with $m = 3$. The crystal structure consists of perovskite type triple-layers which are translated relatively to each other in the basal plane of the unit cell,[4] thereby breaking up the three-dimensional network of corner-sharing CoO_6 octahedra of the perovskite structure. The octahedrally coordinated trivalent cobalt atoms in the perovskite layers suggest the possibility of forming oxygen deficient intermediate phase upon low temperature reduction of $La_4Co_3O_{10}$ analogous to the reduction of $LaCoO_3$.[2,3] The present study focuses on phase relations for $La_4Co_3O_{10-\delta}$, $0.00 \leqslant \delta \leqslant 1.00$, at 673 K. The crystal and magnetic structure of the ordered, reduced phase $La_4Co_3O_9$ has been determined.

Experimental

Synthesis

Samples of nominal compositions $La_4Co_3O_{10-\delta}$ were prepared by isothermal reduction of single phase $La_4Co_3O_{10}$. $La_4Co_3O_{10}$ was obtained after calcination in nitrogen at 1300 K for 110 h.[4] The reduction was performed in sealed silica glass ampoules using Zr as reducing agent (oxygen getter).[2] Phase purity was assured from powder X-ray diffraction. After reaction and equilibration for seven days, all samples were cooled in ice-water. The ampoules were opened in an argon filled glovebox [$p(O_2)$ and $p(H_2O) < 1$ ppm]. Care was taken to assure inert atmosphere during storage, handling and subsequent characterisation of specimens.

Powder diffraction

Room temperature powder X-ray diffraction (PXD) data were collected for all samples with a Guinier-Hägg camera using Si as internal standard ($a = 543.1065$ pm). The sample holders were filled with oil and sealed with Scotch tape on top and bottom. Both $CrK\alpha_1$ (detection limit for impurities *ca.* 0.3 wt%)[5] and $CuK\alpha_1$ radiation were used. The programs TREOR [6] and UNITCELL [7] were used for unit cell indexing and least squares determination of unit cell dimensions. Synchrotron (SR) PXD data were collected for $La_4Co_3O_9$ with the powder diffractometer in Debye–Scherrer mode at the Swiss Norwegian Beam Line (BM1) at ESRF (Grenoble). The sample was contained in a sealed and rotating glass capillary with diameter 0.5 mm. Intensity data were collected at 298 K between $2\theta = 8$ and 70° in steps of $\Delta(2\theta) = 0.007°$, wavelength $\lambda = 110.103$ pm. Powder neutron diffraction (PND) data were collected for $La_4Co_3O_9$ with the two-axis powder diffractometer PUS at the JEEP II reactor, Kjeller (Norway). Intensity data were collected at 10 and 298 K between $2\theta = 10$ and 130°, $\lambda = 153.79$ pm. The steplength between data points was $\Delta(2\theta) = 0.05°$. The GSAS program package[8] was used for combined Rietveld-type profile refinements of powder synchrotron X-ray and neutron diffraction data collected at 298 K. Table 1 summarises characteristic features of the data sets and the variable parameters entering the least-squares refinements. The scattering lengths $b_{La} = 8.27$ fm, $b_{Co} = 2.53$ fm and $b_O = 5.81$ fm were taken from the GSAS library. For profile refinement of the PND data collected at 10 K (crystal and magnetic

Table 1 Characteristic features of the powder synchrotron X-ray (298 K) and neutron diffraction (10, 298 K) data sets for $La_4Co_3O_9$, and list of parameters entering into the Rietveld type refinements

	PXD(SR)		PND	
measured data points	8857		2398	
reflections (*hkl*)	544		790	
λ/pm	110.103		153.79	
scale factor	1		1	
zero point	1		1	
profile parameters	6		3	
unit cell dimensions		3[a]		
positional parameters		25[a]		
isotropic displacement factors		3[a]		
magnetic vector components			(2)[b]	
background coefficients	6		15	
refinable parameters	14	+ 31 +	20	= 65

[a] Common parameters for PXD(SR) and PND in the combined refinements. [b] Only refined for the 10 K data.

structure) the Hewat version[9] of the Rietveld program[10] was used. High temperature PXD data were collected upon continuous heating using a Guinier-Simon camera (Enraf Nonius) and CuKα_1 radiation.

Thermal analysis

Thermogravimetric (TGA) analysis was performed with a Perkin Elmer TGA7. Data reduction was performed with standard programs for the systems.

Magnetic measurements

Magnetic susceptibility data were measured by a Quantum Design SQUID-magnetometer (MPMS) in the temperature range 2–300 K with magnetic fields (H) up to 50.0 kOe (for further experimental details *cf.* ref. 2).

Results and Discussion

Phase relations for $La_4Co_3O_{10-\delta}$, $0.00 \leqslant \delta \leqslant 1.00$

Samples were synthesized with nominal compositions $La_4Co_3O_{10-\delta}$, $0.00 \leqslant \delta \leqslant 1.00$. The compositions $\delta = 0.50$ and 1.00 correspond respectively to the reduction of half (one) and all (two) of the trivalent cobalt atoms in $La_4Co_3O_{10}$. According to PXD at 298 K only two distinct phases occur for $0.00 \leqslant \delta \leqslant 1.00$, namely $La_4Co_3O_{10}$ ($\delta = 0.00$) and $La_4Co_3O_9$ ($\delta = 1.00$). The samples with other nominal compositions, including those with only minor deviation from the stoichiometric compositions $\delta = 0$ and 1, were identified as two phase mixtures, thereby excluding any larger non-stoichiometry for these phases under the present conditions.

The direct phase conversion of $La_4Co_3O_9$ into $La_4Co_3O_{10}$ was verified by oxidation in air using high temperature PXD and TGA. Fig. 1 shows, schematically, the changes in the high temperature PXD pattern of $La_4Co_3O_9$ upon oxidation, heating rate 0.23 K min^{-1}. The sample was subjected to air immediately before starting the experiment. The single phase regimes for $La_4Co_3O_9$ and $La_4Co_3O_{10}$ are separated by a reaction regime at around 320 K where the two phases coexist (shaded background). Fig. 2 shows the weight change upon oxidation of $La_4Co_3O_9$ using TGA. The oxidation rate changes at 400 K after an initial 1% weight increase, which approximately corresponds to $\delta = 0.5$. The higher temperature for the oxidation in the TGA experiment is due to the higher heating rate, 5 K min^{-1}. The weight shows a maximum at approximately 600 K corresponding to the composition $La_4Co_3O_{10.18}$. The maximum is characteristic for the oxidative non-stoichiometry of $La_4Co_3O_{10+\delta}$ when heated in air.[4] PXD of samples oxidized at temperatures below 1250 K verify complete oxidation to $La_4Co_3O_{10+\delta}$. The second weight increase starting above 1250 K corresponds to oxidation of $La_4Co_3O_{10+\delta}$ into a two phase mixture of $LaCoO_3$ and La_2O_3.

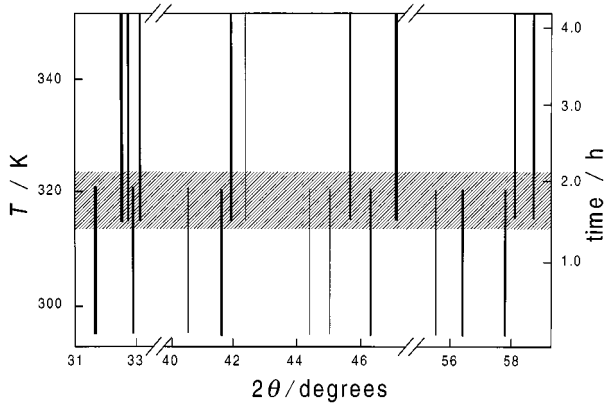

Fig. 1 Schematic representation of parts of the high temperature PXD pattern during oxidation of $La_4Co_3O_9$ in air. Heating rate 0.23 K min^{-1}, $\lambda = 154.06$ pm.

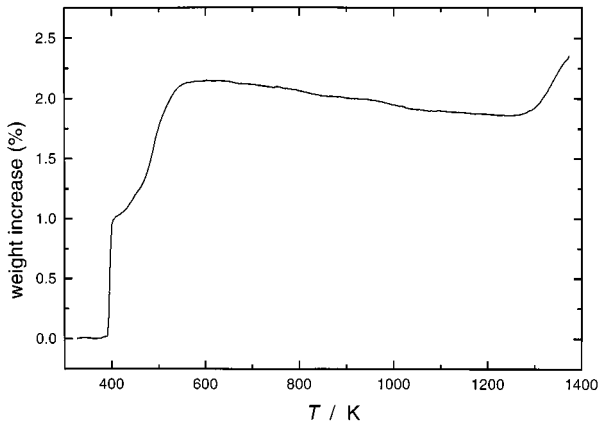

Fig. 2 Thermogravimetric data for oxidation of $La_4Co_3O_9$ in air. Heating rate 5 K min^{-1}.

Crystal structure of $La_4Co_3O_9$

All reflections in the Guinier–Hägg PXD patterns at 298 K for $La_4Co_3O_9$ could be satisfactorily indexed on a primitive orthorhombic unit cell; $a = 545.2(1)$ pm, $b = 2852.1(6)$ pm, $c = 565.5(1)$ pm. The unit cell volume is expanded by 6.9% relative to the unit cell of $La_4Co_3O_{10}$ [space group $C2/m$, $a = 541.79(1)$ pm, $b = 547.56(1)$ pm, $c = 2780.5(1)$ pm, $\beta = 90.200(1)^\circ$][4] and is most prominent along $\bar{b}$ and $\bar{c}$. The volume expansion is mainly caused by the reduction of $Co^{III}(d^6$, low-spin) to the larger sized $Co^{II}(d^7)$. The initial structure model for the profile refinements was based on the Ruddlesden–Popper atomic arrangement for $La_4Co_3O_{10}$ [4] modified by introducing ordered oxygen vacancies in analogy to the reduced phases of $LaCoO_3$, namely $La_2Co_2O_5$ and $La_3Co_3O_8$.[2,3] It was assumed that (*i*) the cationic sublattice is essentially unchanged, (*ii*) the oxygen vacancies are ordered within the triple perovskite layers, resulting in chains of CoO_4 tetrahedra parallel to the shortest unit cell axis, and (*iii*) the displacements of the oxygen atoms and the tetrahedrally coordinated cobalt atoms are similar to those found for $La_2Co_2O_5$ and $La_3Co_3O_8$. The significant differences in the PND patterns between $La_4Co_3O_{10}$ and $La_4Co_3O_9$ indicate that the latter phase can not be considered as a disordered, vacant variant of the former. Considering the well defined peaks in the synchrotron PXD and the PND profiles three possible space groups were indicated, *Pnma*, $A2_1ma$ or $A2_122$. However, a close inspection of the diffraction profiles revealed intensity slightly above the background signal for the reflections; (141), (290), (341), (352) and ($21\bar{3}2$), which should be absent for the space groups $A2_1ma$ and $A2_122$. Hence, the centrosymmetric space group *Pnma* was adopted. The refinements converged satisfactorily and the results of the combined Rietveld refinements of the synchrotron PXD and the PND data are given in Tables 2 and 3. Observed, calculated and difference intensity profiles are shown in Fig. 3.

The crystal structure of $La_4Co_3O_9$ is shown in Fig. 4. The unit cell comprises two triple layers for which the cationic sublattice of $La_4Co_3O_{10}$ is to a large degree preserved during the reduction. Ordering of oxygen vacancies leads to chains of corner-sharing CoO_4 tetrahedra parallel to [100] within the central part of each perovskite type triple layer. The top and bottom part of each triple layer retain the perovskite type arrangement of corner-sharing CoO_6 octahedra. Co(1) and the oxygen atoms are somewhat displaced relative to the atomic positions for $La_4Co_3O_{10}$. Just as for the reduced phase $La_2Co_2O_5$,[2] these displacements and the expansion of $\bar{c}$ reduce the distortions of the CoO_4 tetrahedra and considerable tilting

Table 2 Unit cell data for $La_4Co_3O_9$ and *R*-values. Calculated standard deviations in parentheses

		298 K	10 K
space group		*Pnma*	*Pnma*
a/pm		545.716(5)	543.56(2)
b/pm		2855.33(3)	2846.0(1)
c/pm		565.415(5)	564.67(2)
$V/10^8$pm^3		8.8103(2)	8.7352(7)
Z		4	4
R_p (%)[a]	PXD	4.4	
	PND	7.0	9.8[b]
R_{wp} (%)[a]	PXD	6.2	
	PND	9.0	16.1
R_{exp} (%)[a]	PXD	2.9	
	PND	4.2	10.0
χ^2		4.50	2.60

[a] $R_p = 100(\Sigma|I_o - I_c|/\Sigma I_o)$, $R_{wp} = 100(\Sigma_w(I_o - I_c)^2/\Sigma_w I_o^2)^{-1/2}$, $R_{exp} = R_{wp}/\sqrt{\chi^2}$ according to ref. 8 (298 K) and ref. 9 and 10 (10 K). [b] Combined refinement, crystallographic ($R_N = 9.7\%$) and magnetic ($R_M = 10.6\%$).

Table 3 Fractional atomic coordinates for $La_4Co_3O_9$ at 298 K. Calculated standard deviations in parentheses. Space group *Pnma*. Isotropic displacement factors ($B_{iso}/10^4$pm^2): B_{iso}(La) = 1.92(5), B_{iso}(Co) = 1.02(1), B_{iso}(O) = 0.87(8).

atom	wyckoff site[a]	*x*	*y*	*z*
La(1)	8d	0.250(1)	0.0492(1)	0.9863(6)
La(2)	8d	0.248(1)	0.1724(1)	0.0157(6)
Co(1)	4c	0.212(2)	0.25	0.551(1)
Co(2)	8d	0.251(3)	0.1100(2)	0.500(2)
O(1)	4c	0.353(3)	0.25	0.889(2)
O(2)	8d	0.260(4)	0.0300(3)	0.555(2)
O(3)	8d	0.995(5)	0.1045(3)	0.245(4)
O(4)	8d	0.997(5)	0.1194(3)	0.758(4)
O(5)	8d	0.248(4)	0.1877(3)	0.431(1)

[a] 4c $(x, 1/4, z)$, 8d (x, y, z).

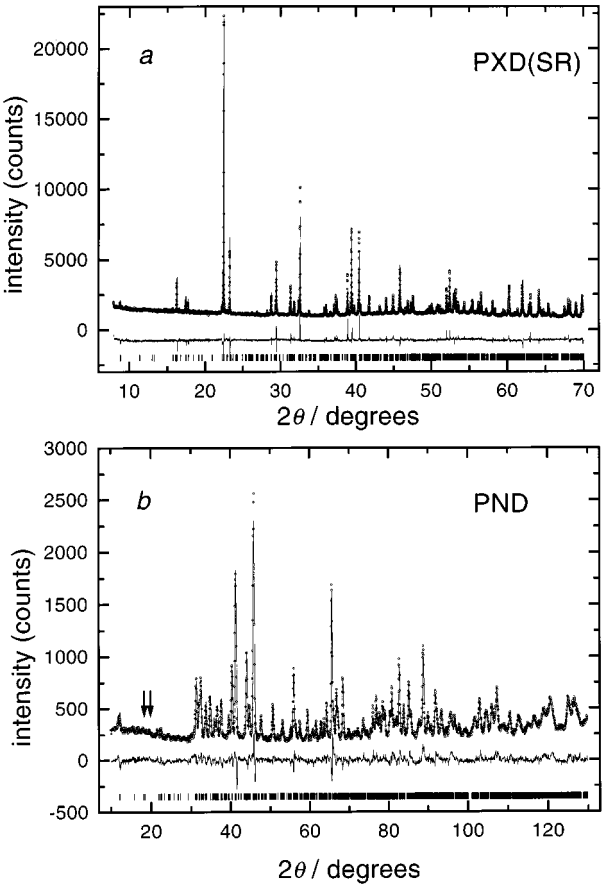

Fig. 3 (*a*) Synchrotron PXD ($\lambda = 110.103$ pm) and (*b*) PND ($\lambda = 153.79$ pm) profiles for $La_4Co_3O_9$ at 298 K. Experimental points marked by open circles, calculated profile by full line; lower full line marks difference plot, vertical bars marks positions for Bragg reflections.

of the CoO_6 octahedra occurs. Despite the atomic displacements there are still considerable distortions of the tetrahedra especially along [010] as shown by the large O(5)—Co(1)—O(5) angle and short Co(1)—O(5) interatomic distances (Table 4). Furthermore, the CoO_6 octahedra are significantly elongated along [010], and the nine fold coordination of oxygen around lanthanum is irregular.

The low temperature reduction of $La_4Co_3O_{10}$ leads to structural changes completely analogous to those accompanying the reduction of $LaCoO_3$ *via* $La_3Co_3O_8$ to $La_2Co_2O_5$. The triple layers in the unit cell of $La_4Co_3O_9$ are separated by layers with NaCl type arrangement of La and O atoms. Hence, for emphasizing such structural building units the chemical formula of $La_4Co_3O_9$ can be rewritten as $LaO(La_3Co_3O_8)$. Similarly $La_4Co_3O_{10}$ can be rewritten as $LaO(LaCoO_3)_3$.

Table 4 Selected interatomic distances (pm) and bond angles (°) for $La_4Co_3O_9$ at 298 K; calculated standard deviations in parentheses, atom numbers refer to Fig. 4

tetrahedron:	Co(1)—O(1)$_1$		206(1)	O(1)$_1$—Co(1)—O(1)$_2$	102.3 (1)
	Co(1)—O(1)$_2$		198(1)	O(1)$_1$—Co(1)—O(5)	106.9 (1)
	Co(1)—O(5)	(×2)	191(1)	O(1)$_2$—Co(1)—O(5)	99.3(1)
				O(5)—Co(1)—O(5)	136.5(1)
octahedron:	Co(2)—O(2)		230(1)	O(2)—Co(2)—O(3)$_1$	92.0(1)
	Co(2)—O(3)$_1$		201(1)	O(2)—Co(2)—O(3)$_2$	90.0(1)
	Co(2)—O(3)$_2$		193(1)	O(2)—Co(2)—O(4)$_1$	92.9(1)
	Co(2)—O(4)$_1$		201(1)	O(2)—Co(2)—O(4)$_2$	91.5(1)
	Co(2)—O(4)$_2$		193(1)	O(5)—Co(2)—O(3)$_1$	86.9(1)
	Co(2)—O(5)		225(1)	O(5)—Co(2)—O(3)$_2$	87.7(1)
				O(5)—Co(2)—O(4)$_1$	89.4(1)
				O(5)—Co(2)—O(4)$_2$	89.5(1)
				O(4)$_1$—Co(2)—O(4)$_2$	87.1(1)
				O(3)$_1$—Co(2)—O(3)$_2$	87.5(1)
				O(3)$_1$—Co(2)—O(4)$_1$	93.0(1)
				O(3)$_2$—Co(2)—O(4)$_2$	92.2(1)
	La(1)—O		230–284, 326(1)	8+1	
	La(2)—O		239–278, 333(1)	8+1	
	polyhedra tilt angles/°				
	Co(1)—O(5)—Co(2)		148.6(1)		
	Co(1)—O(1)—Co(1)		121.8(1)		
	Co(2)—O(3)—Co(2)		170.9(1)		
	Co(2)—O(4)—Co(2)		164.4(1)		

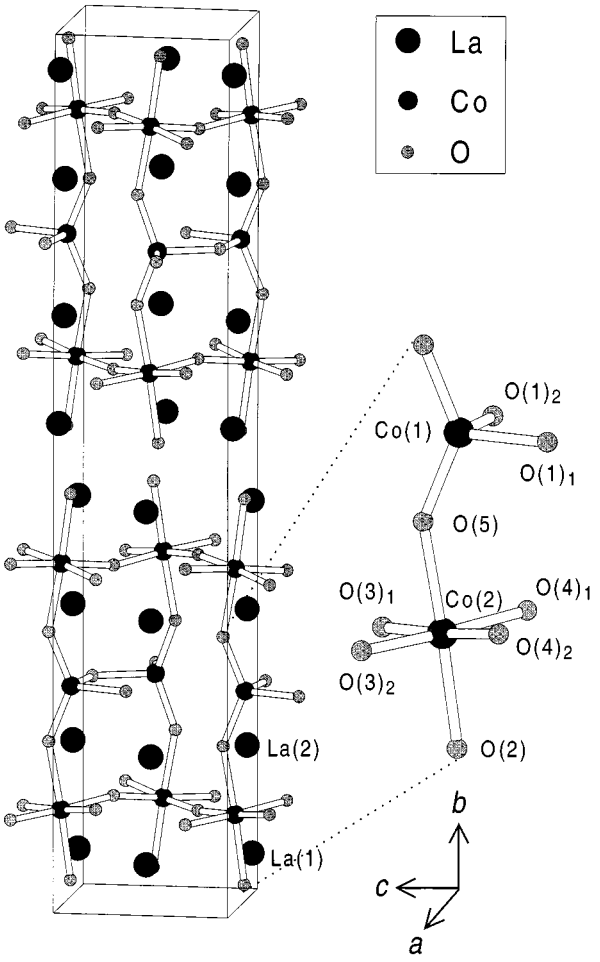

Fig. 4 Crystal structure for $La_4Co_3O_9$. Space group *Pnma*.

Magnetic properties of $La_4Co_3O_9$

The PND data at 10 K showed a number of additional reflections of magnetic origin, see Fig. 5. Their intensities gradually decrease on increasing temperature, with a more pronounced drop above 280 K (Fig. 6). There are still minor magnetic scatterings at 298 K, slightly above the background level, for the reflections (031) and (140), *cf.* arrows in Fig. 3(*b*). The antiferromagnetic ordering temperature $T_N = 303 \pm 5$ K is estimated by extrapolation of the integrated intensity for (031) to the background level (Fig. 6). All additional magnetic reflections (Fig. 5) could be indexed on the crystallographic

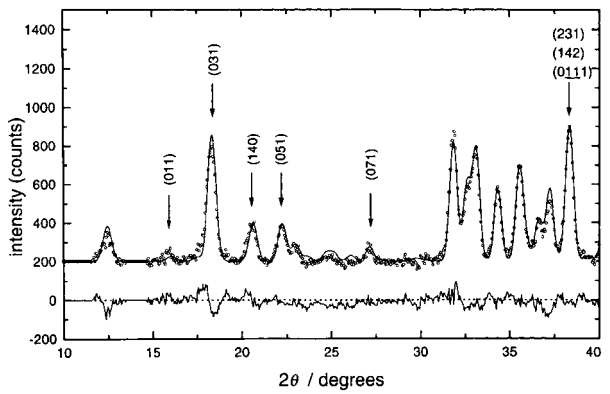

Fig. 5 Selected parts of the PND profile for $La_4Co_3O_9$ at 10 K. Magnetic reflections are marked by arrows and Miller indices are given. Experimental points marked by open circles, full line marks calculated profile, and lower full line marks difference plot. Wavelength $\lambda = 153.79$ pm.

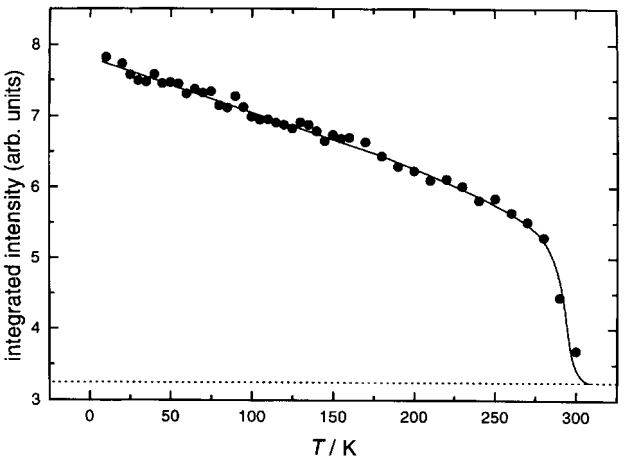

Fig. 6 Temperature dependence of the integrated intensity for the magnetic PND reflection (031). Dashed line represents the background level. Fully drawn line as guide to the eye.

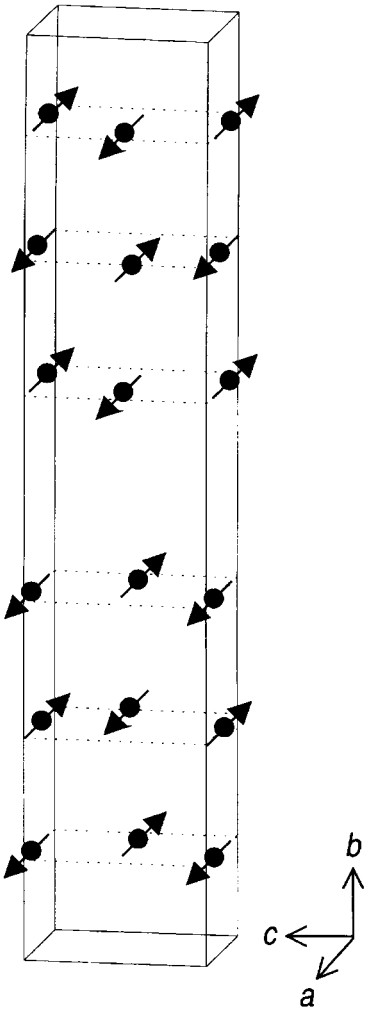

Fig. 7 Antiferromagnetic order in $La_4Co_3O_9$. Only Co atoms shown.

unit cell. The cobalt atoms in the tetrahedra and octahedra are all divalent. All $Co^{II}-O-Co^{II}$ interactions were assumed to be antiferromagnetic in nature. A model of the magnetic structure based on antiferromagnetic ordering of the magnetic moments of all cobalt atoms is proposed. Successive triple layers with G-type ordering arrange as shown in Fig. 7. The refinements gave a reasonable fit to the experimental data, see Fig. 5, with magnetic *R*-value $R_M = 10.6\%$. The refined magnetic moments were $\mu_{tet} = 2.6 \pm 0.1$ μ_B for Co(1) and $\mu_{oct} =$

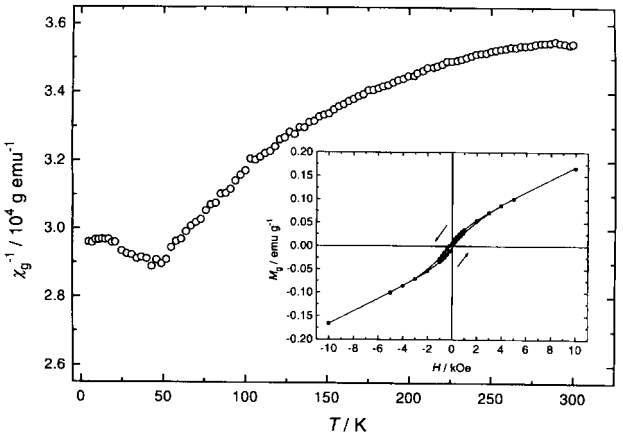

Fig. 8 Temperature dependence of the inverse magnetic susceptibility (χ_g^{-1}) for $La_4Co_3O_9$, measuring field $H=200$ Oe. Inset shows field dependence of the magnetisation (M_g) at 300 K.

3.0 ± 0.1 μ_B for Co(2), both moments oriented parallel to [100]. The magnetic moment values correspond fairly well to that of Co^{II} in the high-spin state ($S=3/2$). The derived magnetic moments for $La_4Co_3O_9$ correspond very well to those obtained for antiferromagnetic $La_2Co_2O_5$ (G-type ordering) with $T_N=301\pm5$ K.[3] The magnetic coupling between successive triple perovskite layers in $La_4Co_3O_9$ is similar to that between single perovskite layers in La_2CoO_4. Note, La_2CoO_4 is the Co^{II}-representative of the Ruddlesden–Popper series $La_{m+1}Co_mO_{3m+1}$ with $m=1$.[11] In La_2CoO_4 antiferromagnetic ordering occurs within the single perovskite layer of octahedrally coordinated Co^{II}, magnetic moment $\mu_{oct}=2.9\pm0.1$ μ_B, $T_N=275$ K. Thus, for the three ternary phases of divalent cobalt in the La–Co–O system, La_2CoO_4, $La_2Co_2O_5$ and $La_4Co_3O_9$, strong antiferromagnetic coupling is present. This feature is typical for high spin Co^{II} in oxides.

A small field hysteresis is observed for the magnetisation, $M_g(H)$, at 298 K (see inset Fig. 8). Since $La_4Co_3O_9$ is antiferromagnetically ordered, it was concluded that the hysteresis most probably is caused by a minor ferromagnetic impurity of metallic cobalt not detectable by PXD. Co(s) may be formed by *e.g.* enhanced surface reduction due to insufficient material equilibration (*i.e.* oxygen diffusion) under the adopted reduction conditions. Other possible causes are a small excess of reducing agent or reduction of minor amounts of cobalt oxide (CoO or Co_3O_4) impurities not detectable by PXD. Similar indications for minor ferromagnetic impurities of cobalt were found for $La_2Co_2O_5$.[3] The magnetic susceptibility, $\chi_g(T)$, of $La_4Co_3O_9$ decreases gradually with temperature for $T>50$ K, but deviates significantly from Curie–Weiss behaviour, Fig. 8. The cusp in $\chi_g^{-1}(T)$ around 50 K could stem from a change in the antiferromagnetic ordering. However, no changes were observed for the integrated intensity of the magnetic PND reflections (Fig. 6). It is, however, likely that the $\chi_g(T)$ curve to a large extent reflects the properties of precipitated Co particles. Depending on the particle size, they will show ferro- or superpara-magnetic behaviour. The cusp at 50 K is possibly related to blocking of superparamagnetic particles.

This work has received financial support from the Research Council of Norway. The skilful assistance from the project team at the Swiss-Norwegian Beam Line, ESRF is gratefully acknowledged. Contribution No 98.5 from the Swiss-Norwegian Beam Line at ESRF.

References

1 C. N. R. Rao, J. Gopalakrishnan and K. Vidyasagar, *Indian J. Chem., Sect. A*, 1984, **23**, 265.
2 O. H. Hansteen, H. Fjellvåg and B. C. Hauback, *J. Mater. Chem.*, 1998, **8**, preceding paper.
3 O. H. Hansteen, H. Fjellvåg and B. C. Hauback, *J. Solid State Chem.*, in press.
4 O. H. Hansteen and H. Fjellvåg, *J. Solid State Chem.*, in press.
5 B. Gilbu, H. Fjellvåg and A. Kjekshus, *Acta Chem. Scand.*, 1994, **48,** 37.
6 P. E. Werner, L. Eriksson and M. Westdahl, Program TREOR (version 5), *J. Appl. Crystallogr.*, 1985, **18**, 367.
7 B. Noläng, Program UNITCELL , Department of Chemistry, Uppsala University, Sweden.
8 A. C. Larson and R. B. Von Dreele, GSAS General Structure Analysis System, LANSCE, MS-H 805, Los Alamos National Laboratory, Los Alamos, NM 87545, USA.
9 A. W. Hewat, Harwell Report RRL 73/239, 1973.
10 H. M. Rietveld, *J. Appl. Crystallogr.*, 1969, **2**, 65.
11 K. Yamada, M. Matsuda, Y. Endoh, B. Keimer, R. J. Birgeneau, S. Onodera, J. Mizusaki, T. Matsuura and G. Shirane, *Phys. Rev. B*, 1989, **39,** 2336.

Paper 8/01798K; *Received* 4*th March*, 1998